

000
001
002
003
004
005
006
007
008
009
010
011054
055
056
057
058
059
060
061
062
063
064
065
066
067
068
069
070
071
072
073
074
075
076
077
078
079
080
081
082
083
084
085
086
087
088
089
090
091
092
093
094
095
096
097
098
099
100
101
102
103
104
105
106
107

Deformable Diversity Similarity for Partial Matching of 3D Shapes

Anonymous CVPR submission

Paper ID ****

Abstract

We propose a novel approach for the matching of partial deformable shapes in 3D. Inspired by recent advances in 2D template matching techniques, our method relies on the concept of deformable diversity similarity(DDIS), extends and adapts it from an image to the 3D shape domain, and leverages the distinct behavior of this framework in different scales to achieve shape correspondences. We evaluate this framework on the SHREC16 partial matching of deformable shapes and show state of the art performance in achieving sparse correspondences.

1. Introduction

Shape correspondence is a fundamental and challenging problem in computer vision and graphics. It has usage in various applications such as transferring texture and animation. Shapes rarely, if ever manifest in only one pose. While rigid transformations between surfaces is a well researched topic with many adequate solutions, a more challenging problem arises when a shape is deformed non-rigidly, a case all too common for people, animals and objects. Moreover, the shape acquisition process almost always lead to partiality of the scanned object. Occlusions arise from different angles of acquisition, which cause an object to occlude itself, or stem from other occluding objects. An additional type of difficulty which might be occur is topological noise, occurring when shapes touch pn another, thus making sensors unable to seperate them. All of these combined give rise to the challenging problem of partial correspondences, where a deformed and incomplete shape, possibly with topological changes, has to be matched with its full version. The goal of this paper is to deal with this challenging problem.

While in a rigid setting the problem can be solved by RANSAC and ICP like approaches[23, 10], extending these to non-rigid case produces mediocre results due to an underlying assumption of small deformations. Early methods specialized for the non-rigid problem focused on minimization of intrinsic metric distortion[6, 32] and regularity of

parts[?, 4]. These methods all contain with them a global assumption of isometry which holds only approximately, these tended to break down with it, and are also unable to handle extreme partiality. Another family of method is based on functional correspondence. These methods model correspondences as a linear operator of a known nature between a space of functions on manifolds[17]. These methods, originally designed for the full shape correspondence scenario have achieved state of the art results on various partial matching tasks in the recent years[14, 33, 21], and produce dense correspondence maps, but are not parallelizable, and their reliance on intrinsic metrics makes them invariant to symmetry.

We take a different approach. We take advantage of the fact that while the isometric property tends to break over large distances, it usually holds approximately in limited environments. These also tend to suffer a lot less from boundary effects, especially when concentrated around the extremities of a shape.

We can thus treat the problem of partial correspondences as matching of multiple templates, each smaller then the partial surface centered around shape landmarks.

In addition, since point descriptors are known to be modified by partiality and deformations, instead of using them directly, we follow the approach off[30](DDIS) which tackles template matching in 2D and use simple statistical assumptions on the nature of nearest neighbors between small patch descriptors, along with the assumption of an approximate conservation of distances in medium environments to obtain similarity scores between these partial shape templates.

We analyze the behavior of DDIS similarity in different scales and devise a multi scale scheme which leverages the advantages of each scale while masking their shortcomings.

We show that using this approach, we are able to generate a set of sparse correspondences, which are less prone to symmetrical assignment than functional correspondence reliant methods, and are of superior quality on the SHREC16 Partial matching challenge[8]. We then demonstrate how these sparse correspondences can be used as an input to existing functional correspondence algorithms to obtain dense

108 correspondences or a higher quality. In summary, our contributions are:
109
110

- 111 • A non trivial extension of Deformable Diversity from
112 2 to 3 Dimensions.
- 113 • A modified DDIS similarity measure which is more
114 well suited to handle matching of templates with a differ-
115 ent number of points.
- 116 • An empirical analysis of DDIS behavior in different
117 scales, leading to an improved multi-scale framework.
- 118 • A novel multi-template approach to partial matching
119 of deformable shapes which can both produce state of
120 the art sparse correspondences, and be used as an input
121 to functional correspondence algorithms, significantly
122 improving the results obtained by these.

123 The rest of the work is organized as follows: in section
124 2 we go over related works in the field of shape analysis.
125 Section 3 introduces our Deformable Diversity framework
126 for 3D shape matching. Experiments and results are given
127 in section 4, and the conclusions are in section 5.

128 2. Related work

129 2.1. Matching Of Deformable Surfaces

130 As a fundamental problem in computer graphics and vi-
131 sion, an extensive body of work have been done on the
132 matching of surfaces. A variety of shape descriptors have
133 been devised for this task which can be roughly divided in
134 to 2 families. Extrinsic ones, such as PFH[24], SHOT[31]
135 and FPFH[23] which are usually calculated in euclidean
136 space and are thus sensitive to non rigid deformations, but
137 can discern between reflections and are also more robust to
138 noise, topological artifacts and boundary effects. On the
139 other hand intrinsic features such as Heat[7] and Wave Ker-
140 nel signatures[2] are invariant under isometric transfor-
141 mations, but are very sensitive to partiality and are unable to
142 discern between symmetric parts. These have been com-
143 monly used to generate rough correspondences between
144 surfaces and point clouds based on their similarity, but are
145 noisy and offer little in terms of bijectivity and continu-
146 ity of the solution. a measure of global consistency using
147 these can be achieved by solving an energy minimization
148 of the disimilarity matrices stemming from an assignment,
149 and the auction algorithm has been commonly employed
150 for this purpose. Other methods use pairwise relations be-
151 tween points such as geodesic distances[26, 27, 28], and
152 search for a configuration which minimizes the distor-
153 tions of these. These methods usually carry a high complexity,
154 both due to calculating the pairwise relations, and the com-
155 binatorial configuration search, and are thus either obtain
156 sparse matches[26, 27, 28] to alleviate this complexity, or

157 used strategies such as coarse to fine solutions. Another
158 common approach has been to embed the shapes into a dif-
159 ferent lower dimension "canonical" space, this has been
160 done by generalized MDS[6], an embedding into the mo-
161 bius group[13], or by representation in the LBO basis[29]
162 A notable family of works are derived from functional cor-
163 respondences. Introduced at[17, 19, 12, 33] these assume
164 that functions can be mapped from one manifold to an-
165 other via a linear operator, finding this transfer operator
166 allows to embed point in a space where the ICP method
167 can obtain correspondences. Lately there has been a large
168 body of works which employ learning methods such as Ran-
169 dom Forests[20] and deep learning architectures[15, 3, 16].
170 These show the promise of achieving state of the art perfor-
171 mance, but require a lot of annotated data.

172 2.2. Partial Matching of Deformable shapes

173 The introduction of partiality adds complications which
174 are not present in the full correspondence scenario. Spectral
175 quantities change drastically, while geodesic paths dis-
176 appear. For the rigid setup, the Iterative Closest Point(ICP)[1]
177 algorithm, preceded by initial alignment[25] tackle partial
178 matching successfully. Adapting this to the rigid setup how-
179 ever has proved to have limited success due to the alignment
180 which is necessary, and thus is only fit for very small non-
181 rigid deformation.

182 Early works which were designed with partial match-
183 ing in mind[4, 5] formulated an energy minimization prob-
184 lem over metric distortion and regularity of correspond-
185 ing parts. Following works relaxed the regularity require-
186 ment by allowing for sparse correspondences[32, 22]. Other
187 works[27, 26] minimized the distortion metric over the
188 shape extremities by doing combinatorial search of least
189 distortion matches and then densify them while employing
190 a refining scheme in the process.

191 In[18] a bag of words point-wise descriptors on a part in
192 conjunction with a constraint on area similarity and the reg-
193 ularity of the boundary length to produce correspondence
194 less matching parts without point to point correspondences
195 by energy minimization.

196 Another line of works employ machine learning tech-
197 niques to learn correspondences between manifolds. Re-
198 cently [21] had proven that partiality induces a slanted di-
199 agonal structure in the correspondence matrix and found
200 the Laplacian eigenfunctions from each basis which induces
201 this structure. Current state of the art[14] uses this notion in
202 conjunction with joint diagonalization. The main drawback
203 of this method, shared with other intrinsic methods, is its
204 invariance to symmetries.

205 3D Shape Descriptors

216 2.3. Template matching in 2D

217 Template matching in 2D is a well researched topic.
 218 Similarly to 3D objects are going complex deformations of
 219 pose, and are only seen partially depending on the camera
 220 point of view. Recently a series of works which use a very
 221 simplistic framework based on the statistical properties of
 222 nearest neighbors in low level feature space had made good
 223 strides in tackling this complex task.

224 **Best Buddies Similarity** Great strides had been
 225 achieved in the field of 2D template matching. Best Buddies
 226 Similarity[9] is a simple framework which employs
 227 a statistical assumption - if two regions \mathcal{N}, \mathcal{M} contain the
 228 same template patches should maintain Bi Directional Similarity.
 229 That is - given a point $n_i \in \mathcal{N}$ and a corresponding
 230 point $m_i \in \mathcal{M}$ they should point to each other as nearest
 231 neighbors - that is if $NN_{\mathcal{M}}(n_i) = m_j$ then on a matching
 232 template we should expect $NN_{\mathcal{N}}(m_j) = n_i$. Solving for a
 233 matching template then amounts to finding the region which
 234 has the highest count of best buddies. This amazingly simple
 235 scheme has been shown to be able to handle occlusions,
 236 missing parts and complex deformations of templates.

237 **Deformable Diversity Similarity** Building upon the
 238 above work, [30] relaxed the requirement for a best buddy
 239 relation, and added a requirement for spatial coherency.

240 The rather cumbersome best buddy relation has been re-
 241 laxed to requiring only that the diversity of the set of nearest
 242 neighbors sets between corresponding templates should be
 243 high. This is actually prerequisite to a high best buddies
 244 similarity score and serves as a rough approximation of it.
 245 For this end diversity is formally defined as:

$$246 \quad DIS = c \cdot |\{n_i \in \mathcal{N} : \exists m_j \in \mathcal{M}, NN(m_j, \mathcal{N}) = n_i\}| \quad (1)$$

247 where $|\cdot|$ denotes group size and $c = 1/\min(|\mathcal{M}|, |\mathcal{N}|)$ is
 248 a normalization factor. Between non corresponding windows,
 249 indeed one should expect most points to have no real
 250 corresponding point, and thus be mapped to a very and re-
 251 mote nearest neighbors. On the other hand, regions contain-
 252 ing matching objects are drawn from the same distribution,
 253 thus the diversity of nearest neighbors should be high. To
 254 accommodate this assumption not only did they reward high
 255 diversity of nearest neighbors, but also penalized map-
 256 ping to the same patch. To this end, another, a negative
 257 diversity measure had been defined:

$$258 \quad \kappa_{\mathcal{M}}(n_i) = |\{m \in \mathcal{M} : NN^a(m, \mathcal{N}) = n_i\}| \quad (2)$$

259 With x_i^a denoting the appearance descriptor of point x_i .
 260 Thus the contribution of a patch $m_j : NN^a(m_j, \mathcal{N}) = n_i$
 261 is $\exp(1 - \kappa_{\mathcal{M}}(n_i))$. An additional observation made has
 262 been that while non isometric deformations do occur, they
 263 should be restricted, small, in real objects. With distance
 264 on the window pixel grid between 2 nearest neighbor points

265 defined as $r_j = d(m_j^l, n_i^l)$ with x_i^l denoting the location
 266 of x_i on a grid, the final Deformable Diversity Similarity
 267 formulation becomes:

$$268 \quad DDIS = c \sum_{\mathcal{N} \rightarrow \mathcal{M}} \frac{1}{1 + r_j} \cdot \exp(1 - \kappa(NN^a(m_j, \mathcal{N}))) \quad (3)$$

269 3. Deformable Diversity for Partial matching 270 of 3D surfaces

271 **1. Goal of this section** In this section we will describe
 272 the application of DDIS framework for matching of partial
 273 deformable shapes.

274 **2. Key ideas of the algorithm** The core of the method lies
 275 in utilizing DDIS as a similarity measure between surface
 276 parts. While partiality and non rigid deformations causes
 277 pointwise descriptors to be inexact, the underlying distri-
 278 bution of the data is still approximately the same for cor-
 279 responding surface patches. As in 2D, correct correspond-
 280 ing points between a template and a matching object should
 281 lie in nearby regions with relation to some reference point
 282 on the template. However, the preservation of distances
 283 holds only approximately even for full template matching,
 284 and even less so in the presence of partiality and topolog-
 285 ical noise. It holds that the longer a distance between 2
 286 points is, the more likely it is that a distortion had occurred
 287 on the geodesic path between them. Thus, instead of us-
 288 ing the entire part for a correspondence between 2 points,
 289 we use a subset of it for the matching. Instead of look-
 290 ing for one central point as done in the original paper, we
 291 sample many points and treat each of them as a separate
 292 template for matching. Thus obtaining better localization.
 293 Even though we do not consider the entire part, and thus do
 294 not enforce global coherency, matches stemming from this
 295 framework are overwhelmingly correct, and this give way
 296 to simple scheme of pruning bad matches. Finally, we ob-
 297 serve that DDIS has different properties at different scales
 298 and thus employ a multi-scale cascade to take advantage of
 299 this fact.

300 **3. Outline of the algorithm (Preprocessing (normal es-
 301 timation, FPFH), Finding the landmark points, computing
 302 DDIS correspondence for pairs, computing correspondence
 303 of surfaces) Include an image of this general overview.**

304 3.1. Algorithm Outline

305 We employ the following pipeline to obtain a sparse set
 306 of correspondences. We begin by finding extremities on
 307 the part \mathcal{N} and use them as anchors for a quasi uniform
 308 sampling of the part. We define a template for each of the
 309 sampled points by extracting a geodesic disk in a defined
 310 radius around it. We calculate point-wise descriptors for
 311 both \mathcal{N}, \mathcal{M} and the induced nearest neighbor field. We
 312 then traverse all the points on \mathcal{M} , calculating deformable
 313 diversity similarity between it and all the query points and

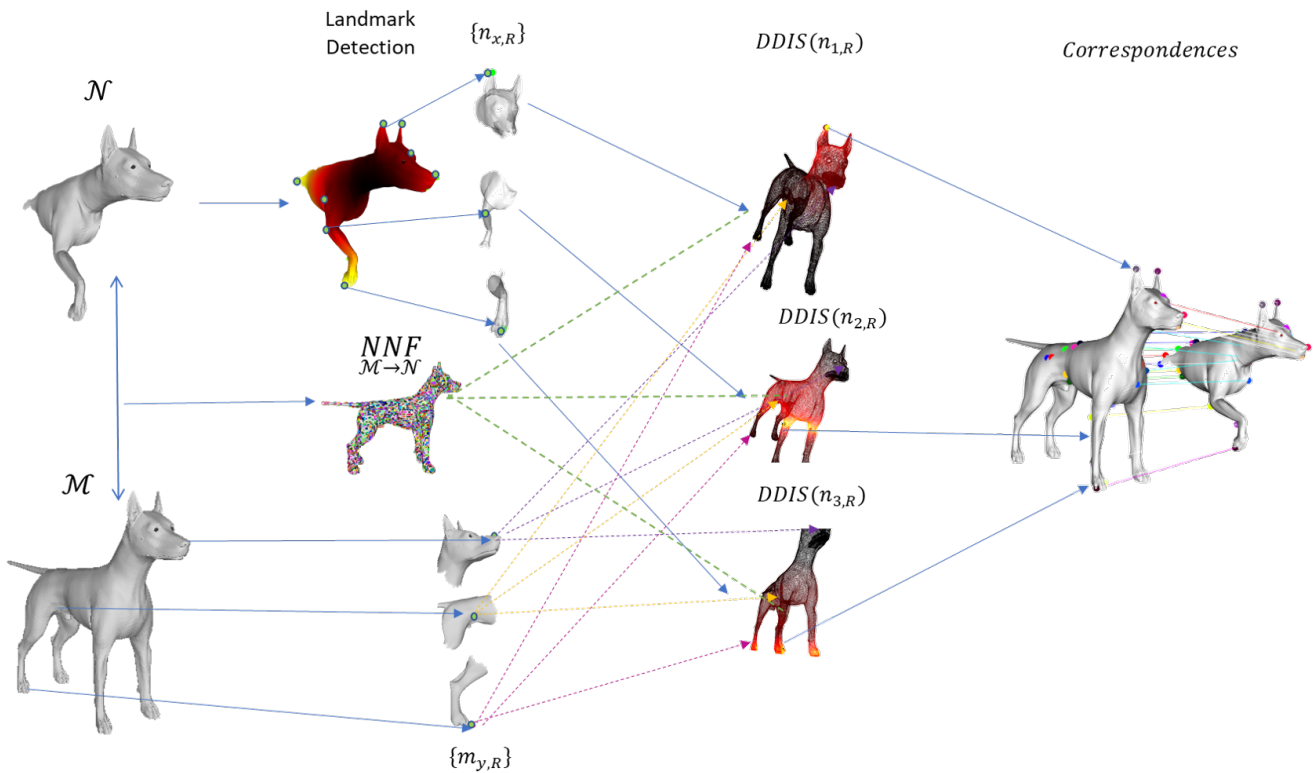


Figure 1. High level illustration of the DDIS Partial Correspondence pipe.

pick the pairs maximizing these as the initial set of correspondences. We then filter out matches which have a high distortion score and use a greedy search for a better match for these from the set of local similarity maximas.

4. Road-map to the section We will begin with a description of the changes made for the deformable diversity framework as a result of moving from 2D to 3D. We will then go over the specific stages of preprocessing necessary for Deformable Diversity in 3D. We will continue with describing the matching process of a single mini template on a full shape. Finally we will describe the extraction of multiple correspondences using this framework.

3.2. Deformable Diversity Similarity in 3D

The nature of 3D data gives rise to unique problems which do not occur in the 2D scenario. Data is distributed in space both sparsely and with varying densities - the amount of data points occupying a given volume can vary drastically. A second problem arises from the absence of a regular grid. These problems require different definitions for key components to the 2D deformable diversity formulation. For this work we chose the image patch to be replaced by a neighborhood which is required to calculate a selected shape descriptor, usually a small sphere in euclidean space or a surface patch with a radius r_F . The search window of a template is defined as a geodesic disc around the query

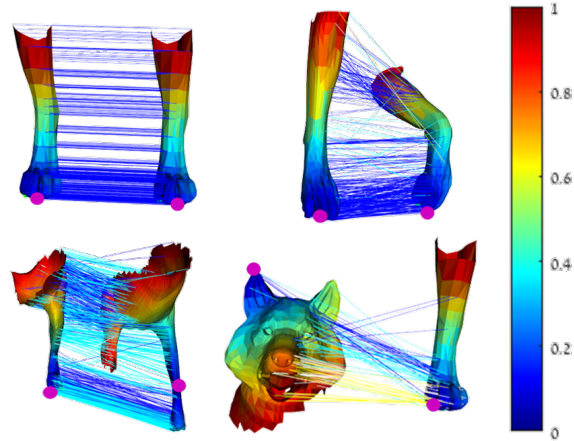


Figure 2. Illustration of Diversity Similarity between different shapes. Geodesic Distances are color coded by the jet scheme. You can notice that on identical pieces, and even on deformed matching pieces there are multiple diverse matches, most of which are colored in blue to indicate very similar distances from the source point, whereas on different pieces most lines map to very few points and a lot of yellow lines (high deformation) exist

point, with a radius denoted by R_T . The pixel grid distance is replaced by either a euclidean distance $d_{Euc}(x^l, y^l)$ (in the

324 378
325 379
326 380
327 381
328 382
329 383
330 384
331 385
332 386
333 387
334 388
335 389
336 390
337 391
338 392
339 393
340 394
341 395
342 396
343 397
344 398
345 399
346 400
347 401
348 402
349 403
350 404
351 405
352 406
353 407
354 408
355 409
356 410
357 411
358 412
359 413
360 414
361 415
362 416
363 417
364 418
365 419
366 420
367 421
368 422
369 423
370 424
371 425
372 426
373 427
374 428
375 429
376 430
377 431

case of point clouds) or geodesic distance $d_{Geo}(x^l, y^l)$ (for surface meshes). Given these DDIS between shape parts \mathcal{M}_{x,R_T} and \mathcal{N}_{y,R_T} can be naively formulated as:

$$DDIS = c \cdot \sum_{m_j \in \mathcal{M}_{x,R_T}} \frac{\exp(1 - \kappa(NN^S(m_j, \mathcal{N}_{y,R_T})))}{1 + r_j} \quad (4)$$

where \mathcal{M}_{x,R_T} and \mathcal{N}_{y,R_T} are the shape parts in a radius R_T surrounding the points $x \in \mathcal{M}$ and $y \in \mathcal{N}$ respectively, r_j is the induced deformation

$$r_j = \frac{|d(m_j^l, m_x^l) - d(NN^S(m_j, \mathcal{N}_{y,R_T})^l, n_y^l)|}{\gamma \cdot R_T} \quad (5)$$

,where γ is a selected fraction and c is a normalization coefficient $c = 1/\min|\mathcal{N}_{y,R_T}|, |\mathcal{M}_{x,R_T}|$.

However, we wouldn't like to penalize our similarity score in case of repeating patterns or symmetrical shapes which have both symmetries in the template search window. Intuitively and empirically the exponent is too harsh and indeed unnecessary as both deformity and diversity will attenuate the score in case of multiple nearest neighbors. On the other hand, we wouldn't want to reward far correspondences at all. **explain why – can we see it visually on the same example? no visual example yet, as the partition into smaller templates mitigates some of the problems of the old formulation it seems, though the new one has still given an extra 2 percent of accurate matches even in the mini template setting**

To account for this the following formulation has been found to work better: given a point $n_i \in \mathcal{N}_{y,R}$ has a set of nearest neighbors in descriptor space on a geodesic disc $\mathcal{M}_{n_i} = \{m_j \in \mathcal{M}_{j,R_T} : NN^S(m_j, N_{y,R_T}) = n_i\}$, we define $m'_i = \operatorname{argmin}_{m_j \in \mathcal{M}_{n_i}}(r_j)$ and r'_i the minimal distortion distance, we add only the contribution of this point to the similarity score which then becomes

$$DDIS(\mathcal{N}_{y,R_T}, \mathcal{M}_{x,R_T}, \gamma) = \sum_{m'_i} \frac{1}{1 + r'_i} \quad (6)$$

This equation still promotes both diversity and low deformations, but is less biased toward surfaces which are either symmetrical, or exhibit repeating patterns.

3.3. DDIS Template Matching

Goal of the algorithm In this section we go over the flow of template matching of 3D shapes using DDIS, the solution of which constitutes the core of our partial shape matching. Given a template \mathcal{N}_{y,R_T} with a reference point n_y as its center and a maximal distance R_T , we aim to find on a model \mathcal{M} which has a deformed version of it, the corresponding surface piece \mathcal{M}_{y^*,R_T} and its center m_{y^*} .

The solution is obtained by finding the point on \mathcal{M} whose surrounding geodesic disc maximizes the above mentioned DDIS measure. **key ideas**

Overview We'll first give an overview, and then give an extended description of each of each stage.

We start by calculating the normals for \mathcal{M} and \mathcal{N} . We than calculate local point descriptors for each patch of some neighborhood around the points in each mesh(For our purpose FPFH seemed to work the best of our tested descriptors). Having calculated these, we calculate a nearest neighbor field by finding for each patch in \mathcal{M} it's Nearest Neighbor in \mathcal{N} . We now find the distance of every point $n \in \mathcal{N}$ to the desired point $y \in \mathcal{N}$ for a desired neighborhood R_T . We now go over every point $x \in \mathcal{M}$. For each we extract the geodesic disc \mathcal{M}_{x,R_T} around it. We take notice that while the above stages are done here in the context of template matching for one template, when matching multiple templates all of the above calculations have to be done only once between the shapes, with the exception of geodesic distance field extraction for the template itself. Finally we calculate DDIS for this disc with $\mathcal{N}_{y,R}$ which has y as its center. Having done that for every point, the point $y^* \in \mathcal{M}$ which gets the maximal DDIS Score is deemed the corresponding point to y .

Point Normal Estimation There are various schemes for estimating point normals given a triangulated mesh surface. We have picked the one which is available in the standard PCL. Given a vertex p_i on a triangulated mesh \mathcal{X} and its associated polygons $\{A_j\}_{j=1}^k$ and their normals N_{A_j} the point normal $N_i = \sum_{j=1}^k |A_j| \cdot N_{A_j}$

Local Patch Size choice DDIS as defined by [30] uses patch descriptors as low level features for their similarity measure. While a patch in an image can by defined by the images grid no such grid exists on 3D point clouds and meshes, where density of data points can vary. Thus a patch has to be defined by some geometric measure. While the more robust way to define it would be using geodesic distance, since we are talking a small environment around a point on the mesh we have found that for practical purposes a patch in a defined euclidean radius r_F around a point serves well enough. We pick this radius in the following way: given the full surface mesh \mathcal{M} we find its equivalent of a diameter $D_{\mathcal{M}} = \sqrt{\operatorname{Area}(\mathcal{M})}$, and tune a parameter α to obtain $r_F = \frac{\alpha}{*} D_{\mathcal{M}}$

Local Patch Descriptor A lot of local shape descriptors have been used successfully in 3D shape analysis. We have tested the following descriptors which are included in the Point Cloud Library: ROPS[?, Theorem 2] PFH[] SHOT[], HKS[], SIHKS[], ROPS[] and FPFH[]. Out of these 4 FPFH has achieved the best performance, and thus the descriptor for the local patch has been chosen to be FPFH.

Nearest Neighbor Field As an intermediate stage towards the calculation of Deformable Diversity Simi-

486
487
488
489
490
491
492
493
494
495
496
497
498
499
500
501
502
503
504
505
506
507
508
509
510
511
512
513
514
515
516
517
518
519
520
521
522
523
524
525
526
527
528
529
530
531
532
533
534
535
536
537
538
539

540 larity measure, the calculation of the nearest neighbor
 541 field(will be abbreviated as NNF) needs to be calculated.
 542 Thus for every patch $m \in \mathcal{M}$ we have to
 543 find the patch on the template $n \in \mathcal{N}$ which resem-
 544 bles it the most. For $FPFH, NN^S(m_j, \mathcal{N})$ is defined
 545 $NN^S(m_j, \mathcal{N}) \equiv \underset{i}{\operatorname{argmin}} \chi^2(FPFH(m_j], FPFH(n_i))$
 546 and the Nearest Neighbor Field is the set of all these cor-
 547 respondences.

548 **DDIS calculation** For every point in $m_x \in \mathcal{M}$ we then
 549 extract a surface part $\mathcal{M}_{x,R}$ with a radius R arund it and
 550 calculate deformable diversity around it. The point which
 551 maximizes DDIS gives us a correspondence (n_y, m_y*) .
 552 Since as we will show in the results section, imperfections
 553 in the isometry assumption lead to considerable localization
 554 errors, we move to a multiple template matching framework
 555 using DDIS, as will be described in the next section.

556 3.4. DDIS Sparse Correspondences

557 A key takeaway from experimenting with DDIS as a
 558 template matching algorithm for partial matching has been
 559 that isometry does not hold, at least not globally. It does
 560 however, hold pretty well locally, especially at extremities.
 561 To this end we devise multiple template framework for Par-
 562 tial correspondences of deformable shape. We first obtain
 563 the landmarks $F = \{f\}_i$ as described in []. We then choose
 564 a partiality radius $R = \gamma \cdot R$ and extract surface parts $\mathcal{N}_{i,R}$
 565 around each extremity point. Finally for each point we cal-
 566 culate DDIS to get it's correspondence.

567 **Landmark Extraction** We follow the work of [Sagi
 568 Katz Ayellet Tal] to obtain interesting landmark points.
 569 Given a shape the work employs the following framework
 570 to extract it's extremities. A point is detected as an extre-
 571 mity if it fulfills 2 conditions: - it's sum of geodesic distances
 572 is a local extrema, formally, for $v \in S$, where S is a surface
 573 mesh, we define the set of points with a direct edge to it as
 574 N_v , the point is a critical point if :

$$\sum_{v_i \in S} d_{geo}(v, v_i) > \sum_{v_i \in S} d_{geo}(v_n, v_i), \forall v_n \in N_v \quad (7)$$

575 An additional requirement for it to be an extremities is for
 576 it to lie on the convex hull of the shape's MDS. In this work
 577 we have dropped the last condition, but chose N_v* - a neigh-
 578 borhood of $0.03 \cdot \sqrt{\text{Area}(S)}$.

579 **Landmark Template Matching** For this end, we create
 580 a template for each landmark point - we collect all surface
 581 point in a geodesic neighborhood around it of $\beta \cdot \sqrt{\text{area}(\mathcal{M})}$
 582 where for this case a good β (0.2, 0.5) where larger beta
 583 prevents global scale error, such as a cats paw being mapped
 584 to a hind paw, while smaller beta promotes tighter localiza-
 585 tion on the part itself. This can be seen in Figure[] While it
 586 might seem natural to calculate a different nearest neighbor
 587 field for each landmark template it has been empirically
 588 found that using the global nearest neighbor field gives

Algorithm 1 3DIS Sparse Correspondences	594
procedure DDIS CORRESPONDENCE($\mathcal{M}, \mathcal{N}, \alpha, \beta, \gamma$) \triangleright Returns point correspondence for critical points on \mathcal{N}	595
$r_F \leftarrow \alpha / 100 \cdot \sqrt{\text{Area}(\mathcal{M})}$ $R_{thresh} \leftarrow \beta / 100 \cdot \sqrt{\text{Area}(\mathcal{M})}$ $N_{\mathcal{M}} \leftarrow \text{ComputeNormals}(\mathcal{M})$ $N_{\mathcal{N}} \leftarrow \text{ComputeNormals}(\mathcal{N})$ $F_{\mathcal{M}} \leftarrow FPFH(\mathcal{M}, N_{\mathcal{M}}, r_F)$ $F_{\mathcal{N}} \leftarrow FPFH(\mathcal{N}, N_{\mathcal{N}}, r_F)$ $NNF_{\mathcal{M} \rightarrow \mathcal{N}} \leftarrow ANN(F_{\mathcal{M}}, F_{\mathcal{N}})$ $\mathcal{N}_c = \{n : \sum_{n_i \in \mathcal{N}} d_{geo}(n, n_i) > 0.03 \cdot \sqrt{\text{Area}(\mathcal{M})}\}$ $\text{for } n_y \in \mathcal{N}_c \text{ do} \quad \triangleright \text{DDIS calculation Loop}$ $m_{c*} \leftarrow DDIS_Correspondence(\mathcal{M}, n_y, \mathcal{N}, \alpha, \beta, \gamma)$ end for $\text{return } \mathcal{M}_c \times \mathcal{N}_c = \{m_{c*}, n_c\}$	596
end procedure	597

598 much better results. This is probably due to the fact that the
 599 nearest neighbor field encodes global information when ob-
 600 tained this way and eliminates local distractors. Each land-
 601 mark template is compared to all surface parts of a similar
 602 R on \mathcal{M} to obtain final point correspondences.

603 3.5. Cascaded Multi-Scale DDIS

604 The observation of the effects of the choice of β and the
 605 trade-off between finer localization and avoidance of global
 606 errors naturally leads to the adoption of a multi scale frame-
 607 work. We calculate *DDIS* score for multiple *beta* values,
 608 and use the location obtained with a large beta to select a
 609 narrow environment in which we look for the maximum
 610 of DDIS with a smaller value *beta*, thus using the larger
 611 scale to get a rough global location, and the smaller scale
 612 to fit it into a more exact location. While this might be
 613 done at multiple custom scales we have found that the triplet
 614 $\beta, 2 \cdot \beta / 3, \beta / 3$ works well.

615 4. Experiments and results

616 In this section we will briefly go over the experiments
 617 performed and their results. We'll introduce the datasets,
 618 detail our experiments and their results

619 4.1. Datasets

620 In this section we will briefly go over the available
 621 Datasets

622 4.1.1 SHREC 2016

623 The SHREC partial matching dataset consists of 8 base,
 624 neutral pose models: cat, centaur, dog, horse, wolf, and

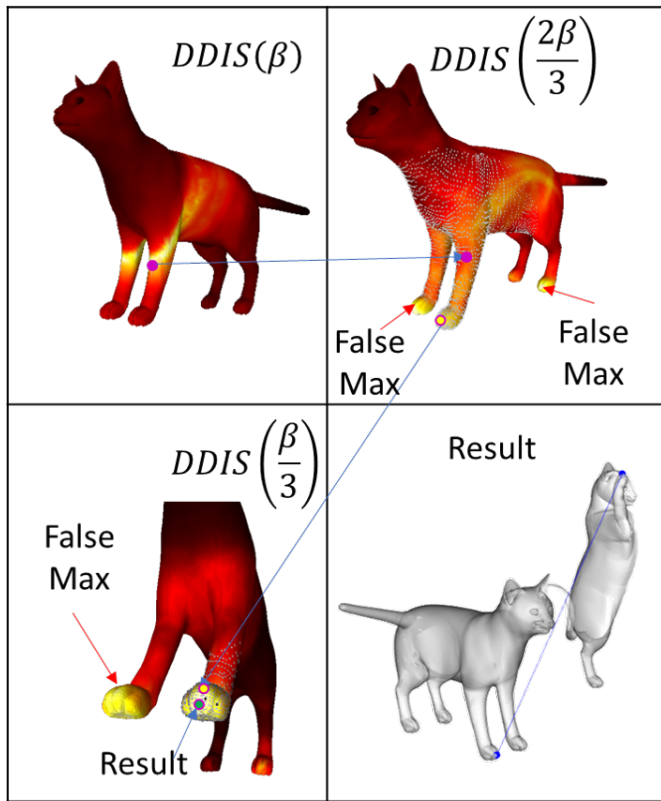


Figure 3. Illustration of the multi scale framework. Gray point are the area chosen by the previous scale to be valid. It can be seen that Wrong maxima in lower scales are ignored due to this process

3 humans 2 males, and 1 female. Each basic model has corresponding deformed partial shapes obtained either by cutting the shape with a plane or by adding holes on a deformed shape. The set has been divided into train and test sets. The train set is composed of 15 cuts for each base models totaling 120 models, and 10 holed shpaes for each model for which ground truth point to polygon correspondences has been provided in barycentric coordinates. The test set is composed of additional 200 cuts and 200 holed shapes.

4.2. Error Metrics

The output of partial matching algorithms (as defined in[8]) are sub-vertex point-to-point correspondences between partial shapes. For all experiments we use the standard practice of not penalizing symmetric solutions. Quality is measured according to the Princeton benchmark protocol [11]. For a pair of points $(x, y) \in \mathcal{N} \times \mathcal{M}$ between the full object \mathcal{M} and the partial shape \mathcal{N} produced by an algorithm, where (x, y^*) is the ground truth correspondence

the inaccuracy is measured by

$$\varepsilon(x) = \frac{d_{\mathcal{M}}(y, y^*)}{\sqrt{\text{area}(\mathcal{M})}} \quad (8)$$

where $d_{\mathcal{M}}(y, y^*)$ is the geodesic distance on \mathcal{M} , and has units of normalized length on \mathcal{M} . For dense correspondences over a dataset, $\varepsilon(x)$ is averaged over all matching instances.

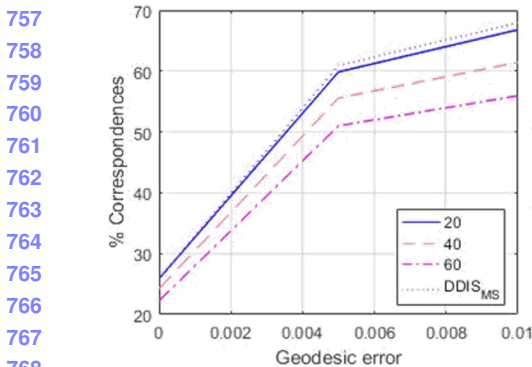
4.2.1 Central Points Localization

In this experiment we have chosen for each Template mesh the center point c_T and tried to match it to a point on the object using DDIS. Experiments have been done using FPFH, PFH and SHOT as patch descriptors with patch radiiuses of $[2, 3, 4, 5]$, the results of the opimal parameter for each descriptor are illustrated in fig. and visualizations of similarity maps of cuts are provided in fig. . It can be seen that good localization is obtained for points on a smooth surface, under high partiality conditions and strong deformations. Bad matches occur when a matched point resides on a heavily deformed patch, and when salient anchor points are deformed or cut. Analysis of these results shows a drift in localization occurs when salient features are divided by strong unisometric deformations which serve as the motivation for the multiple template matching framework.

4.3. Sparse Correspondences on the SHREC16 Test set

In this experiment we have tested the performance of DDIS in producing sparse correspondences on the SHREC16 Partial Matching of Deformable Shapes competition. We had tuned our parameters on the SHREC16 training dataset using only the cuts part of it. The best results had been produced using FPFH with $r_F = 0.04\sqrt{\text{Area}(\mathcal{M})}$, and a piece size radius $R_{thresh} = 0.3\sqrt{\text{Area}(\mathcal{M})}$. For Geodesic distances we have found the fast marching algorithm to work the fastest, while giving the lowest error w.r.t. to exact geodesics. For a 10,000 vertices mesh it takes 60s to produce a full distance matrix, Though it should be noted this algorithm has a more efficient GPU implementation. FPFH and Nearest Neighbor field takes 2 s' and similarity between 2 pieces of 10000 vertices each takes 25s on average, running on a single thread of i7-2700k. Unlike optimization based algorithms this is highly parallelizable. We achieve results comparable to the state of the art [14] quality wise, even though sparser in nature on both the Cuts and the Holes datasets, Where a particularly impressive result is reported on the Holes dataset. A further look reveals even more reliable results can be obtained taking only the extremity points not lying on the mesh longest boundary, but they will be more sparse

756



757

758

759

760

761

762

763

764

765

766

767

768

769

770

771

772

773

774

775

776

777

778

779

780

781

782

783

784

785

786

787

788

789

790

791

792

793

794

795

796

797

798

799

800

801

802

803

804

805

806

807

808

809

810

811

812

813

814

815

816

817

818

819

820

821

822

823

824

825

826

827

828

829

830

831

832

833

834

835

836

837

838

839

840

841

842

843

844

845

846

847

848

849

850

851

852

853

854

855

856

857

858

859

860

861

862

863

Figure 4. Effect of the β parameter on the results: it can be seen that a smaller beta promotes better localization in a small neighborhood, while higher values of β lead to more local errors but are more robust to global errors. It can be seen that the multi-scale cascade achieves better results both locally and globally.

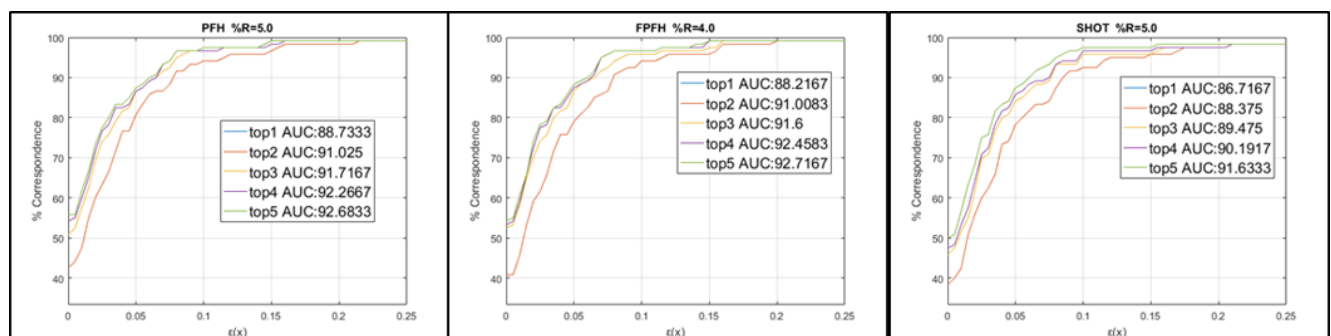


Figure 5. Comparison between descriptors: we show curves for the minimal distance of the top results. a noticeable addition occurs when adding the 2nd best match

Table 1. mean number of correspondence obtained by the algorithms in the SHREC 16 competition and our algorithm

References

- [1] D. Aiger, N. J. Mitra, and D. Cohen-Or. 4pointss congruent sets for robust pairwise surface registration. *ACM Trans. Graph.*, 27(3):85:1–85:10, Aug. 2008. 2
- [2] M. Aubry, U. Schlickewei, and D. Cremers. The wave kernel signature: A quantum mechanical approach to shape analysis. In *Computer Vision Workshops (ICCV Workshops), 2011 IEEE International Conference on*, pages 1626–1633. IEEE, 2011. 2
- [3] D. Boscaini, J. Masci, E. Rodolà, and M. Bronstein. Learning shape correspondence with anisotropic convolutional neural networks. In *Advances in Neural Information Processing Systems*, pages 3189–3197, 2016. 2
- [4] A. M. Bronstein and M. M. Bronstein. Not only size matters: regularized partial matching of nonrigid shapes. In *Computer Vision and Pattern Recognition Workshops, 2008. CVPRW'08. IEEE Computer Society Conference on*, pages 1–8. IEEE, 2008. 1, 2
- [5] A. M. Bronstein, M. M. Bronstein, A. M. Bruckstein, and R. Kimmel. Partial similarity of objects, or how to compare a centaur to a horse. *International Journal of Computer Vision*, 84(2):163, 2009. 2
- [6] A. M. Bronstein, M. M. Bronstein, and R. Kimmel. Generalized multidimensional scaling: a framework for isometry-invariant partial surface matching. *Proceedings of the National Academy of Sciences*, 103(5):1168–1172, 2006. 1, 2
- [7] M. M. Bronstein and I. Kokkinos. Scale-invariant heat kernel signatures for non-rigid shape recognition. In *Computer Vision and Pattern Recognition (CVPR), 2010 IEEE Conference on*, pages 1704–1711. IEEE, 2010. 2
- [8] L. Cosmo, E. Rodolà, M. Bronstein, A. Torsello, D. Cremers, and Y. Sahillioglu. Shrec16: Partial matching of deformable shapes. *Proc. 3DOR*, 2, 2016. 1, 7
- [9] T. Dekel, S. Oron, M. Rubinstein, S. Avidan, and W. T. Freeman. Best-buddies similarity for robust template matching. In *Proceedings of the IEEE Conference on Computer Vision and Pattern Recognition*, pages 2021–2029, 2015. 3
- [10] D. Holz, A. E. Ichim, F. Tombari, R. B. Rusu, and S. Behnke. Registration with the point cloud library: A modular framework for aligning in 3-d. *IEEE Robotics & Automation Magazine*, 22(4):110–124, 2015. 1

864

865

866

867

868

869

870

871

872

873

874

875

876

877

878

879

880

881

882

883

884

885

886

887

888

889

890

891

892

893

894

895

896

897

898

899

900

901

902

903

904

905

906

907

908

909

910

911

912

913

914

915

916

917

918

919

920

921

922

923

924

925

926

927

928

929

930

931

932

933

934

935

936

937

938

939

940

941

942

943

944

945

946

947

948

949

950

951

952

953

954

955

956

957

958

959

960

961

962

963

964

965

966

967

968

969

970

971

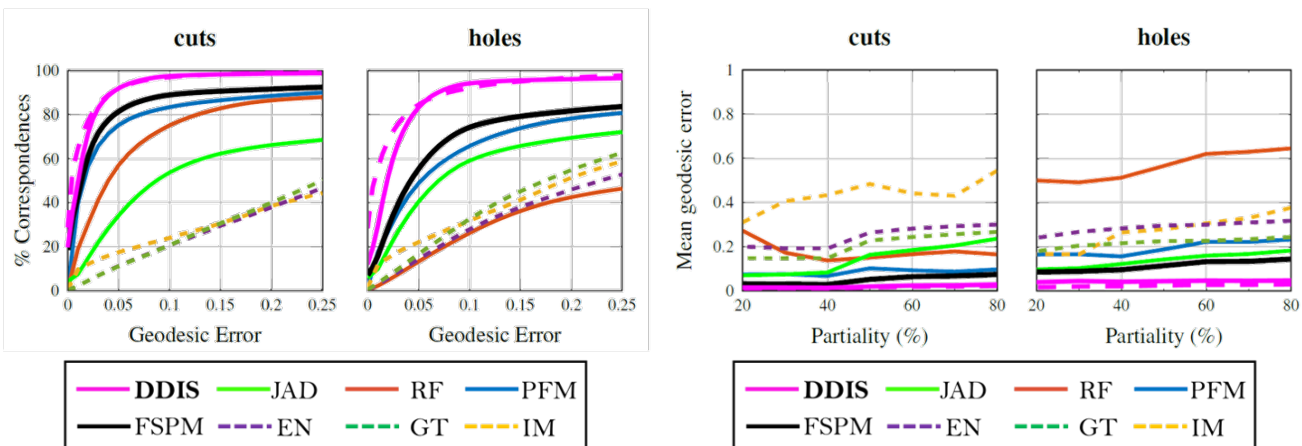


Figure 6. comparison with other state of the art algorithms - it can be seen that although sparse in nature, the correspondence obtained by DDIS are much more accurate than the other methods. A separate analysis has been done for correspondences which include boundary points, which tend to be more noisy, and internal points which are more sparse

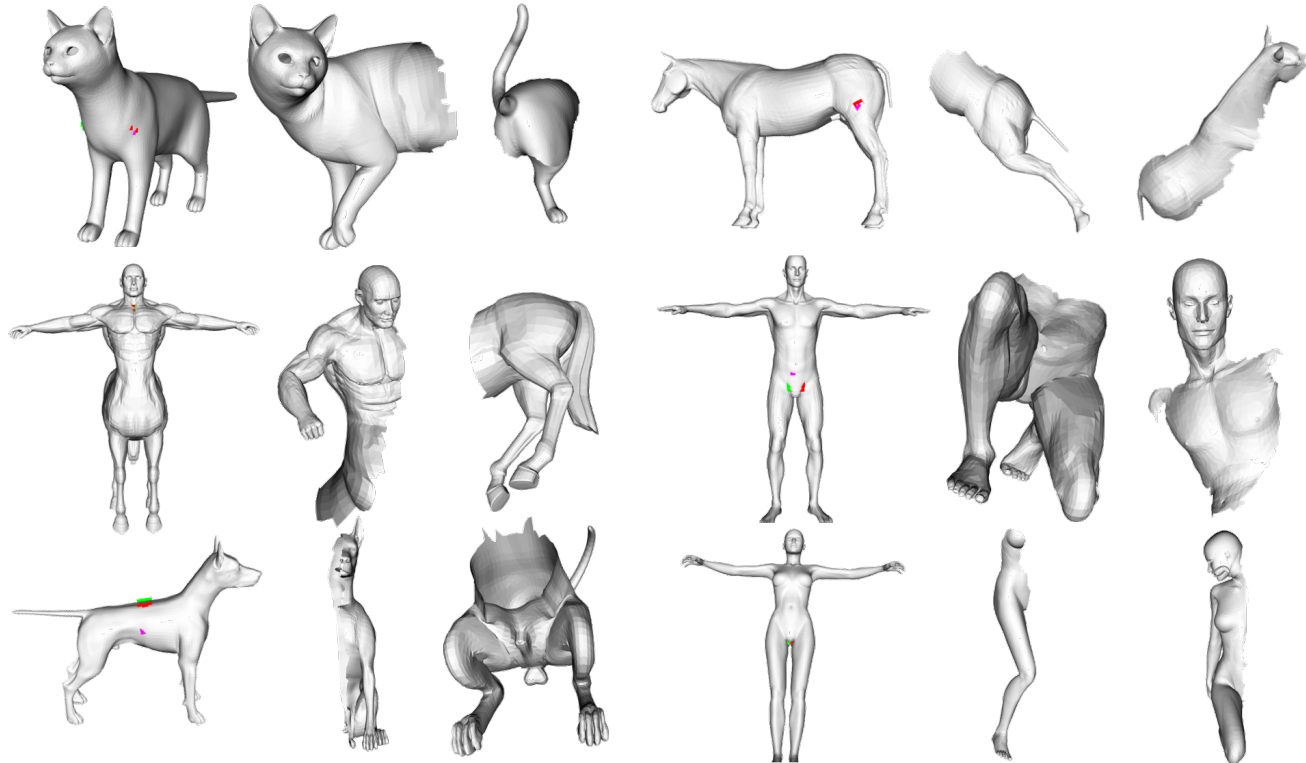


Figure 7. SHREC 16 cuts partial matching dataset.

- [11] V. G. Kim, Y. Lipman, and T. Funkhouser. Blended intrinsic maps. In *ACM Transactions on Graphics (TOG)*, volume 30, page 79. ACM, 2011. 7
- [12] A. Kovnatsky, M. M. Bronstein, X. Bresson, and P. Vandergheynst. Functional correspondence by matrix completion. In *Proceedings of the IEEE conference on computer vision and pattern recognition*, pages 905–914, 2015. 2
- [13] Y. Lipman and T. Funkhouser. Möbius voting for surface

correspondence. *ACM Transactions on Graphics (TOG)*, 28(3):72, 2009. 2

- [14] O. Litany, E. Rodolà, A. M. Bronstein, and M. M. Bronstein. Fully spectral partial shape matching. In *Computer Graphics Forum*, volume 36, pages 247–258. Wiley Online Library, 2017. 1, 2, 7
- [15] J. Masci, E. Rodolà, D. Boscaini, M. M. Bronstein, and H. Li. Geometric deep learning. In *SIGGRAPH ASIA 2016*

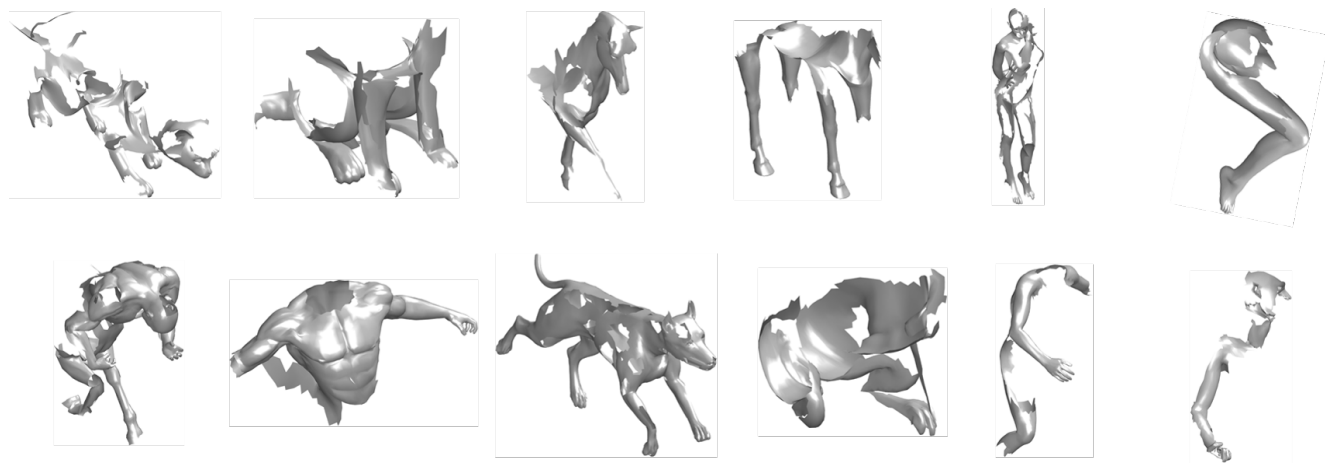


Figure 8. SHREC 16 holes partial matching dataset.

Courses, page 1. ACM, 2016. 2

- [16] F. Monti, D. Boscaini, and J. Masci. Geometric deep learning on graphs and manifolds using mixture model cnns. 2
- [17] M. Ovsjanikov, M. Ben-Chen, J. Solomon, A. Butscher, and L. Guibas. Functional maps: A flexible representation of maps between shapes. *ACM Trans. Graph.*, 31(4):30:1–30:11, July 2012. 1, 2
- [18] J. Pokrass, A. M. Bronstein, and M. M. Bronstein. Partial shape matching without point-wise correspondence. *Numerical Mathematics: Theory, Methods and Applications*, 6(1):223–244, 2013. 2
- [19] J. Pokrass, A. M. Bronstein, M. M. Bronstein, P. Sprechmann, and G. Sapiro. Sparse modeling of intrinsic correspondences. In *Computer Graphics Forum*, volume 32, pages 459–468. Wiley Online Library, 2013. 2
- [20] E. Rodolà, S. R. Bulò, T. Windheuser, M. Vestner, and D. Cremers. Dense non-rigid shape correspondence using random forests. In *Proceedings of the 2014 IEEE Conference on Computer Vision and Pattern Recognition, CVPR ’14*, pages 4177–4184, Washington, DC, USA, 2014. IEEE Computer Society. 2
- [21] E. Rodolà, L. Cosmo, M. M. Bronstein, A. Torsello, and D. Cremers. Partial functional correspondence. In *Computer Graphics Forum*, volume 36, pages 222–236. Wiley Online Library, 2017. 1, 2
- [22] E. Rodola, A. Torsello, T. Harada, Y. Kuniyoshi, and D. Cremers. Elastic net constraints for shape matching. In *Proceedings of the IEEE International Conference on Computer Vision*, pages 1169–1176, 2013. 2
- [23] R. B. Rusu, N. Blodow, and M. Beetz. Fast point feature histograms (fpfh) for 3d registration. In *Robotics and Automation, 2009. ICRA’09. IEEE International Conference on*, pages 3212–3217. Citeseer, 2009. 1, 2
- [24] R. B. Rusu, Z. C. Marton, N. Blodow, and M. Beetz. Learning informative point classes for the acquisition of object model maps. In *Control, Automation, Robotics and Vision, 2008. ICARCV 2008. 10th International Conference on*, pages 643–650. IEEE, 2008. 2

- [25] R. B. Rusu, Z. C. Marton, N. Blodow, M. Dolha, and M. Beetz. Towards 3d point cloud based object maps for household environments. *Robotics and Autonomous Systems*, 56(11):927–941, 2008. 2
- [26] Y. Sahillioğlu and Y. Yemez. Minimum-distortion isometric shape correspondence using em algorithm. *IEEE transactions on pattern analysis and machine intelligence*, 34(11):2203–2215, 2012. 2
- [27] Y. Sahillioğlu and Y. Yemez. Scale normalization for isometric shape matching. In *Computer Graphics Forum*, volume 31, pages 2233–2240. Wiley Online Library, 2012. 2
- [28] Y. Sahillioglu and Y. Yemez. Coarse-to-fine combinatorial matching for dense isometric shape correspondence. In *Computer Graphics Forum*, volume 30, pages 1461–1470. Wiley Online Library, 2011. 2
- [29] A. Shtern and R. Kimmel. Matching the lbo eigenspace of non-rigid shapes via high order statistics. *Axioms*, 3(3):300–319, 2014. 2
- [30] I. Talmi, R. Mechrez, and L. Zelnik-Manor. Template matching with deformable diversity similarity. In *Proc. of IEEE Conf. on Computer Vision and Pattern Recognition*, pages 1311–1319, 2017. 1, 3, 5
- [31] F. Tombari, S. Salti, and L. Di Stefano. Unique signatures of histograms for local surface description. In *European conference on computer vision*, pages 356–369. Springer, 2010. 2
- [32] A. Torsello. A game-theoretic approach to deformable shape matching. In *Proceedings of the 2012 IEEE Conference on Computer Vision and Pattern Recognition (CVPR), CVPR ’12*, pages 182–189, Washington, DC, USA, 2012. IEEE Computer Society. 1, 2
- [33] M. Vestner, Z. Lähner, A. Boyarski, O. Litany, R. Slossberg, T. Remez, E. Rodola, A. Bronstein, M. Bronstein, R. Kimmel, et al. Efficient deformable shape correspondence via kernel matching. In *3D Vision (3DV), 2017 International Conference on*, pages 517–526. IEEE, 2017. 1, 2

1080

References

1081

1082

1083

1084

1085

1086

1087

1088

1089

1090

1091

1092

1093

1094

1095

1096

1097

1098

1099

1100

1101

1102

1103

1104

1105

1106

1107

1108

1109

1110

1111

1112

1113

1114

1115

1116

1117

1118

1119

1120

1121

1122

1123

1124

1125

1126

1127

1128

1129

1130

1131

1132

1133

- [1] D. Aiger, N. J. Mitra, and D. Cohen-Or. 4pointss congruent sets for robust pairwise surface registration. *ACM Trans. Graph.*, 27(3):85:1–85:10, Aug. 2008. 2
- [2] M. Aubry, U. Schlickewei, and D. Cremers. The wave kernel signature: A quantum mechanical approach to shape analysis. In *Computer Vision Workshops (ICCV Workshops), 2011 IEEE International Conference on*, pages 1626–1633. IEEE, 2011. 2
- [3] D. Boscaini, J. Masci, E. Rodolà, and M. Bronstein. Learning shape correspondence with anisotropic convolutional neural networks. In *Advances in Neural Information Processing Systems*, pages 3189–3197, 2016. 2
- [4] A. M. Bronstein and M. M. Bronstein. Not only size matters: regularized partial matching of nonrigid shapes. In *Computer Vision and Pattern Recognition Workshops, 2008. CVPRW’08. IEEE Computer Society Conference on*, pages 1–6. IEEE, 2008. 1, 2
- [5] A. M. Bronstein, M. M. Bronstein, A. M. Bruckstein, and R. Kimmel. Partial similarity of objects, or how to compare a centaur to a horse. *International Journal of Computer Vision*, 84(2):163, 2009. 2
- [6] A. M. Bronstein, M. M. Bronstein, and R. Kimmel. Generalized multidimensional scaling: a framework for isometry-invariant partial surface matching. *Proceedings of the National Academy of Sciences*, 103(5):1168–1172, 2006. 1, 2
- [7] M. M. Bronstein and I. Kokkinos. Scale-invariant heat kernel signatures for non-rigid shape recognition. In *Computer Vision and Pattern Recognition (CVPR), 2010 IEEE Conference on*, pages 1704–1711. IEEE, 2010. 2
- [8] L. Cosmo, E. Rodolà, M. Bronstein, A. Torsello, D. Cremers, and Y. Sahillioglu. Shrec16: Partial matching of deformable shapes. *Proc. 3DOR*, 2, 2016. 1, 7
- [9] T. Dekel, S. Oron, M. Rubinstein, S. Avidan, and W. T. Freeman. Best-buddies similarity for robust template matching. In *Proceedings of the IEEE Conference on Computer Vision and Pattern Recognition*, pages 2021–2029, 2015. 3
- [10] D. Holz, A. E. Ichim, F. Tombari, R. B. Rusu, and S. Behnke. Registration with the point cloud library: A modular framework for aligning in 3-d. *IEEE Robotics & Automation Magazine*, 22(4):110–124, 2015. 1
- [11] V. G. Kim, Y. Lipman, and T. Funkhouser. Blended intrinsic maps. In *ACM Transactions on Graphics (TOG)*, volume 30, page 79. ACM, 2011. 7
- [12] A. Kovnatsky, M. M. Bronstein, X. Bresson, and P. Vandergheynst. Functional correspondence by matrix completion. In *Proceedings of the IEEE conference on computer vision and pattern recognition*, pages 905–914, 2015. 2
- [13] Y. Lipman and T. Funkhouser. Möbius voting for surface correspondence. *ACM Transactions on Graphics (TOG)*, 28(3):72, 2009. 2
- [14] O. Litany, E. Rodolà, A. M. Bronstein, and M. M. Bronstein. Fully spectral partial shape matching. In *Computer Graphics Forum*, volume 36, pages 247–258. Wiley Online Library, 2017. 1, 2, 7
- [15] J. Masci, E. Rodolà, D. Boscaini, M. M. Bronstein, and H. Li. Geometric deep learning. In *SIGGRAPH ASIA 2016 Courses*, page 1. ACM, 2016. 2
- [16] F. Monti, D. Boscaini, and J. Masci. Geometric deep learning on graphs and manifolds using mixture model cnns. 2
- [17] M. Ovsjanikov, M. Ben-Chen, J. Solomon, A. Butscher, and L. Guibas. Functional maps: A flexible representation of maps between shapes. *ACM Trans. Graph.*, 31(4):30:1–30:11, July 2012. 1, 2
- [18] J. Pokrass, A. M. Bronstein, and M. M. Bronstein. Partial shape matching without point-wise correspondence. *Numerical Mathematics: Theory, Methods and Applications*, 6(1):223–244, 2013. 2
- [19] J. Pokrass, A. M. Bronstein, M. M. Bronstein, P. Sprechmann, and G. Sapiro. Sparse modeling of intrinsic correspondences. In *Computer Graphics Forum*, volume 32, pages 459–468. Wiley Online Library, 2013. 2
- [20] E. Rodolà, S. R. Bulò, T. Windheuser, M. Vestner, and D. Cremers. Dense non-rigid shape correspondence using random forests. In *Proceedings of the 2014 IEEE Conference on Computer Vision and Pattern Recognition, CVPR ’14*, pages 4177–4184, Washington, DC, USA, 2014. IEEE Computer Society. 2
- [21] E. Rodolà, L. Cosmo, M. M. Bronstein, A. Torsello, and D. Cremers. Partial functional correspondence. In *Computer Graphics Forum*, volume 36, pages 222–236. Wiley Online Library, 2017. 1, 2
- [22] E. Rodola, A. Torsello, T. Harada, Y. Kuniiyoshi, and D. Cremers. Elastic net constraints for shape matching. In *Proceedings of the IEEE International Conference on Computer Vision*, pages 1169–1176, 2013. 2
- [23] R. B. Rusu, N. Blodow, and M. Beetz. Fast point feature histograms (fpfh) for 3d registration. In *Robotics and Automation, 2009. ICRA’09. IEEE International Conference on*, pages 3212–3217. Citeseer, 2009. 1, 2
- [24] R. B. Rusu, Z. C. Marton, N. Blodow, and M. Beetz. Learning informative point classes for the acquisition of object model maps. In *Control, Automation, Robotics and Vision, 2008. ICARCV 2008. 10th International Conference on*, pages 643–650. IEEE, 2008. 2
- [25] R. B. Rusu, Z. C. Marton, N. Blodow, M. Dolha, and M. Beetz. Towards 3d point cloud based object maps for household environments. *Robotics and Autonomous Systems*, 56(11):927–941, 2008. 2
- [26] Y. Sahillioglu and Y. Yemez. Minimum-distortion isometric shape correspondence using em algorithm. *IEEE transactions on pattern analysis and machine intelligence*, 34(11):2203–2215, 2012. 2
- [27] Y. Sahillioglu and Y. Yemez. Scale normalization for isometric shape matching. In *Computer Graphics Forum*, volume 31, pages 2233–2240. Wiley Online Library, 2012. 2
- [28] Y. Sahillioglu and Y. Yemez. Coarse-to-fine combinatorial matching for dense isometric shape correspondence. In *Computer Graphics Forum*, volume 30, pages 1461–1470. Wiley Online Library, 2011. 2
- [29] A. Shtern and R. Kimmel. Matching the lbo eigenspace of non-rigid shapes via high order statistics. *Axioms*, 3(3):300–319, 2014. 2

- 1188 [30] I. Talmi, R. Mechrez, and L. Zelnik-Manor. Template match- 1242
1189 ing with deformable diversity similarity. In *Proc. of IEEE 1243
1190 Conf. on Computer Vision and Pattern Recognition*, pages 1244
1191 1311–1319, 2017. 1, 3, 5 1245
1192 [31] F. Tombari, S. Salti, and L. Di Stefano. Unique signatures of 1246
1193 histograms for local surface description. In *European con- 1247
1194 ference on computer vision*, pages 356–369. Springer, 2010. 1248
1195 2 1249
1196 [32] A. Torsello. A game-theoretic approach to deformable shape 1250
1197 matching. In *Proceedings of the 2012 IEEE Conference on 1251
1198 Computer Vision and Pattern Recognition (CVPR)*, CVPR 1252
1199 ’12, pages 182–189, Washington, DC, USA, 2012. IEEE 1253
1200 Computer Society. 1, 2 1254
1201 [33] M. Vestner, Z. Lähner, A. Boyarski, O. Litany, R. Slossberg, 1255
1202 T. Remez, E. Rodola, A. Bronstein, M. Bronstein, R. Kim- 1256
1203 mel, et al. Efficient deformable shape correspondence via 1257
1204 kernel matching. In *3D Vision (3DV), 2017 International 1258
1205 Conference on*, pages 517–526. IEEE, 2017. 1, 2 1259
1206
1207
1208
1209
1210
1211
1212
1213
1214
1215
1216
1217
1218
1219
1220
1221
1222
1223
1224
1225
1226
1227
1228
1229
1230
1231
1232
1233
1234
1235
1236
1237
1238
1239
1240
1241

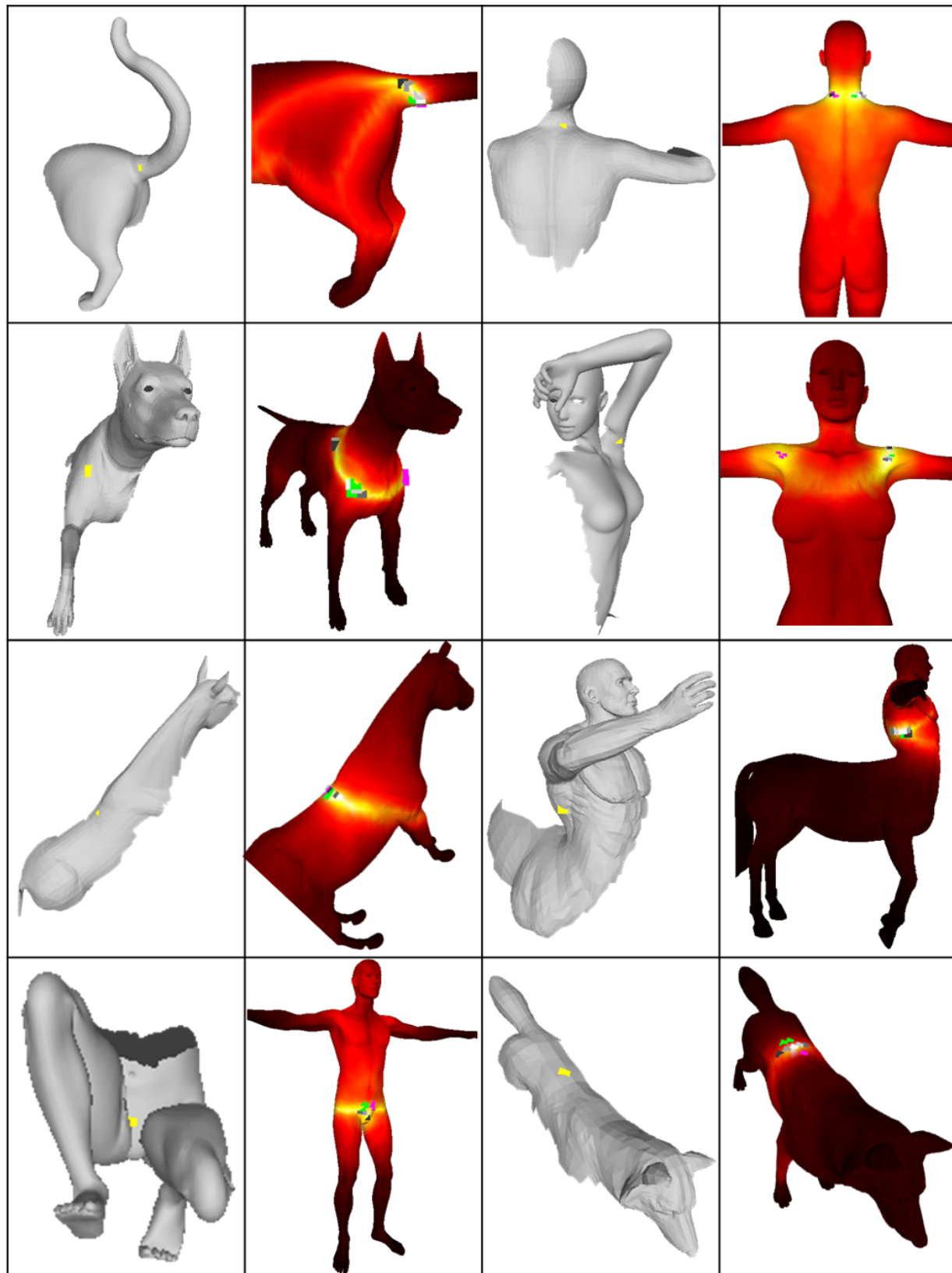
1296
1297
1298
1299
1300
1301
1302
1303
1304
1305
1306
1307
13081309
1310
1311
1312
1313
1314
1315
1316
1317
1318
1319
1320
13211350
1351
1352
1353
1354
1355
1356
1357
1358
1359
1360
1361
13621322
1323
1324
1325
1326
1327
1328
1329
1330
1331
1332
1333
1334
1335
1336
1337
1338
1339
1340
1341
1342
1343
1344
1345
1346
13471363
1364
1365
1366
1367
1368
1369
1370
1371
1372
1373
1374
1375

Figure 9. Some examples of cuts and their matching similarity score maps. The compared point is marked in yellow on the cut, whereas ground truth polygon is marked in green, symmetrical polygon in purple, and top 5 matches in grayscale

1376
1377
1378
1379
1380
1381
1382
1383
1384
1385
1386
1387
1388
1389
1390
1391
1392
1393
1394
1395
1396
1397
1398
1399
1400
1401
1402
1403

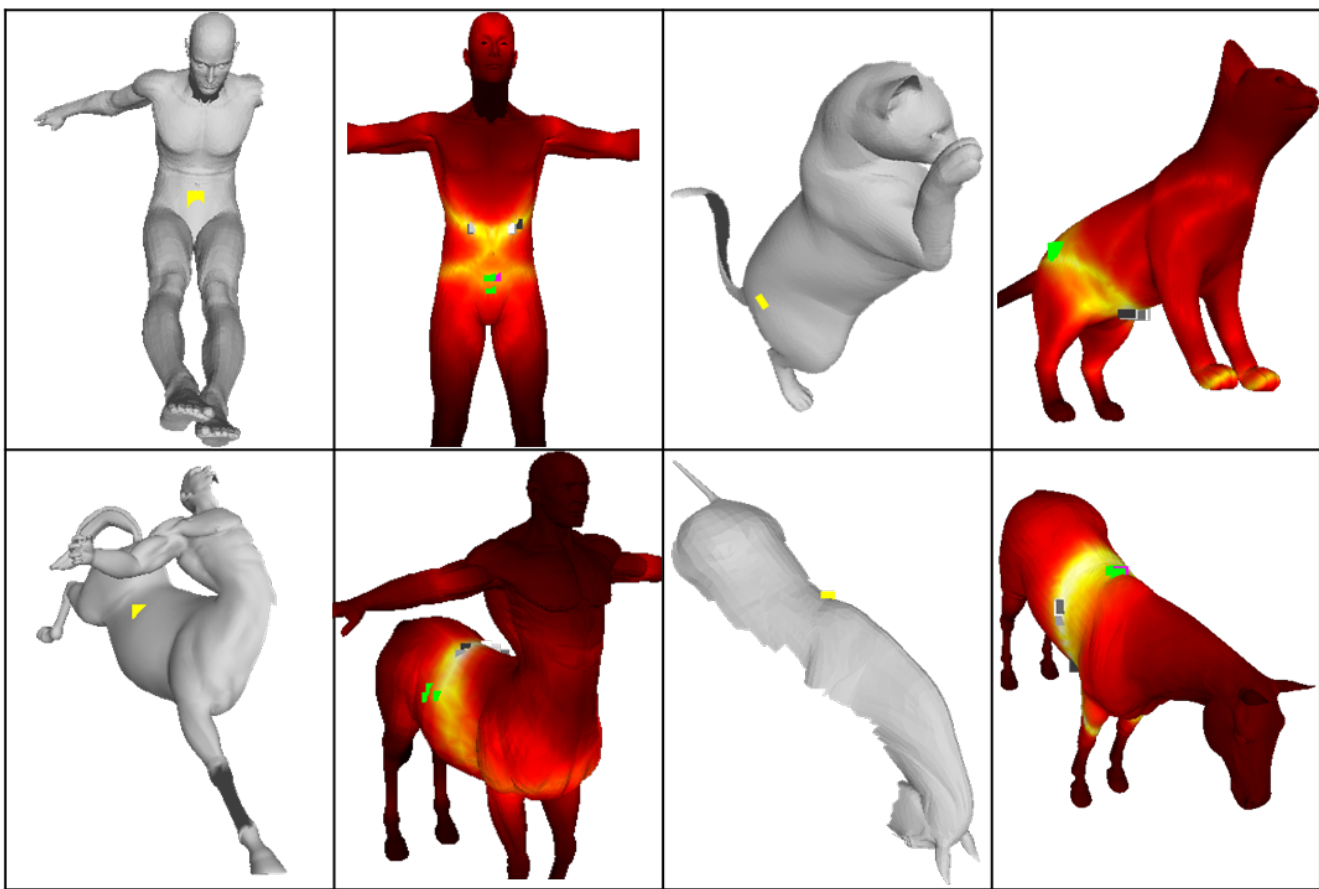
1404
1405
1406
1407
1408
1409
1410
1411
1412
1413
1414
1415
1416
1417
1418
1419
14201421
1422
1423
1424
1425
1426
1427
1428
1429
1430
1431
1432
1433
1434
1435
1436
1437
1438
1439
1440
1441
1442
1443
1444
1445
1446
1447
1448
1449
1450
1451
1452
1453
1454
1455
1456
1457
1458
1459
1460
1461
1462
1463
1464
1465
1466
1467
1468
1469
1470
1471
1472
1473
1474
1475
1476
1477
1478
1479
1480
1481
1482
1483
1484
1485
1486
1487
1488
1489
1490
1491
1492
1493
1494
1495
1496
1497
1498
1499
1500
1501
1502
1503
1504
1505
1506
1507
1508
1509
1510
1511

Figure 10. Some notable failure cases: (1)The man's abdomen is unisometrically deformed (2)The cats

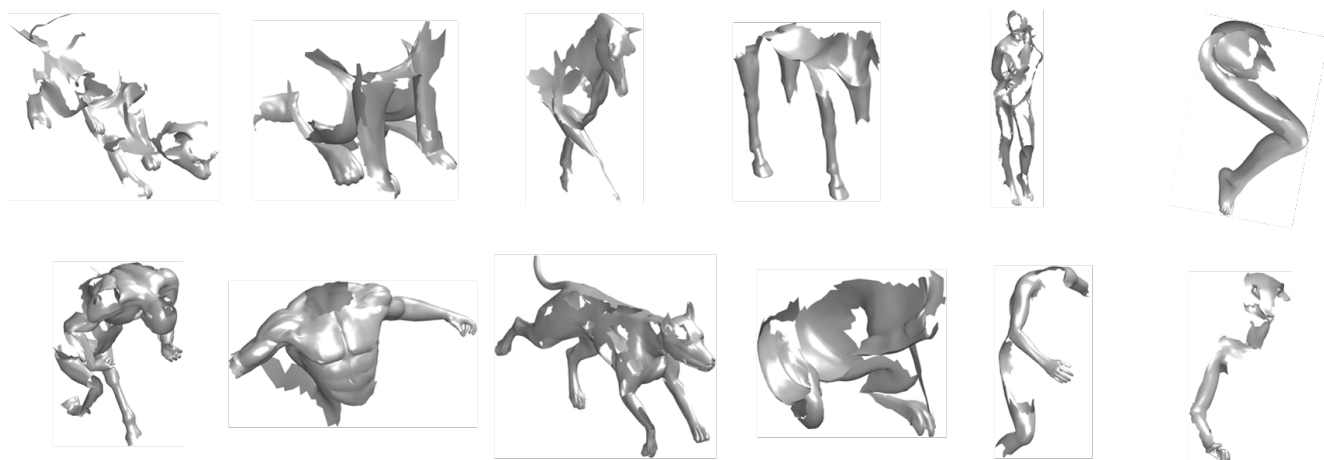


Figure 11. SHREC 16 holes partial matching dataset.

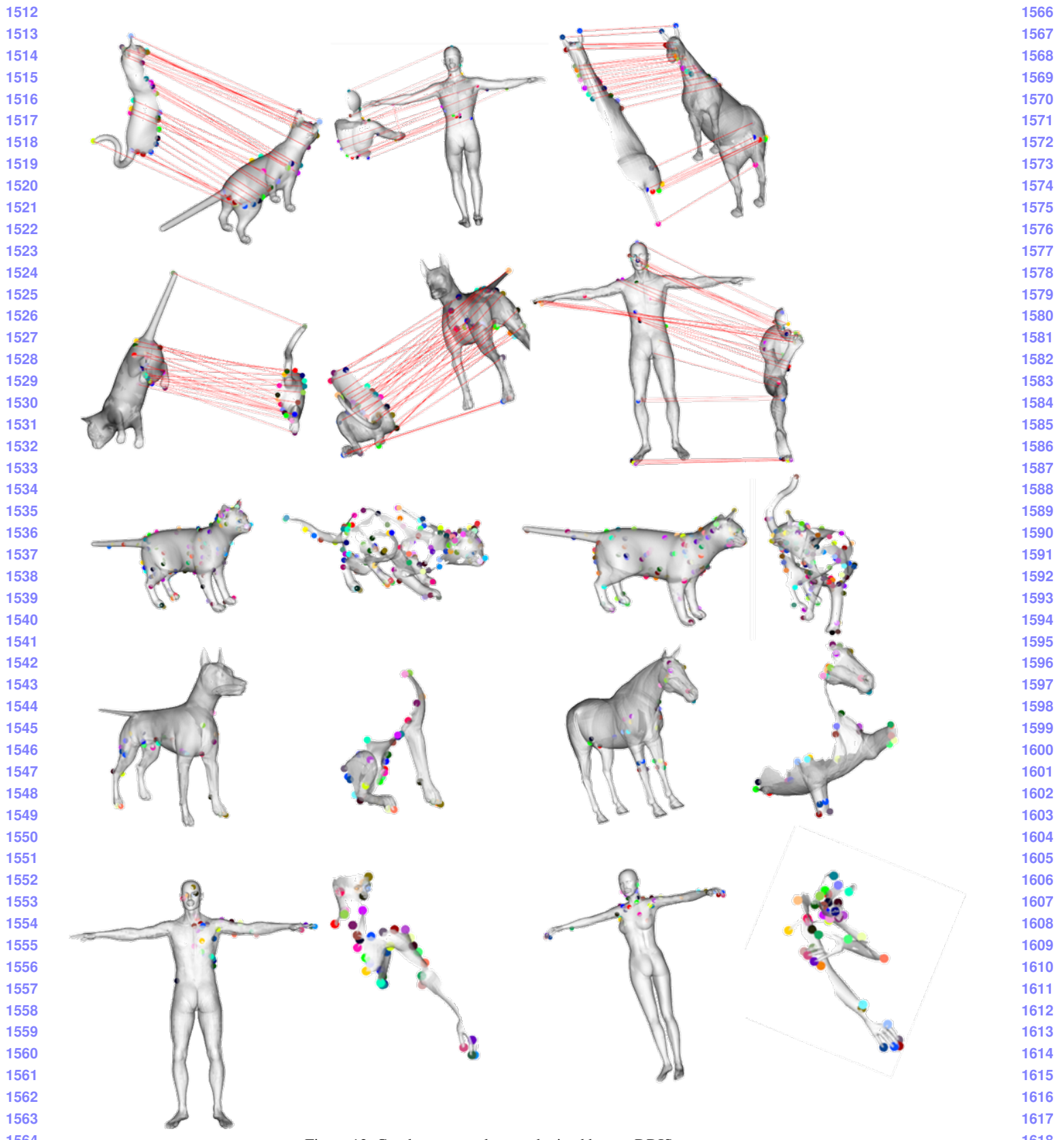


Figure 12. Good correspondences obtained by our DDIS measure

1620
1621
1622
1623
1624
1625
1626
1627
1628
1629
1630
1631
1632
1633
1634
1635
1636
1637
1638
1639
1640
1641
1642
1643
1644
1645
1646
1647
1648
1649
1650
1651
1652
1653
1654
1655
1656
1657
1658
1659
1660
1661
1662
1663
1664
1665
1666
1667
1668
1669
1670
1671
1672
1673

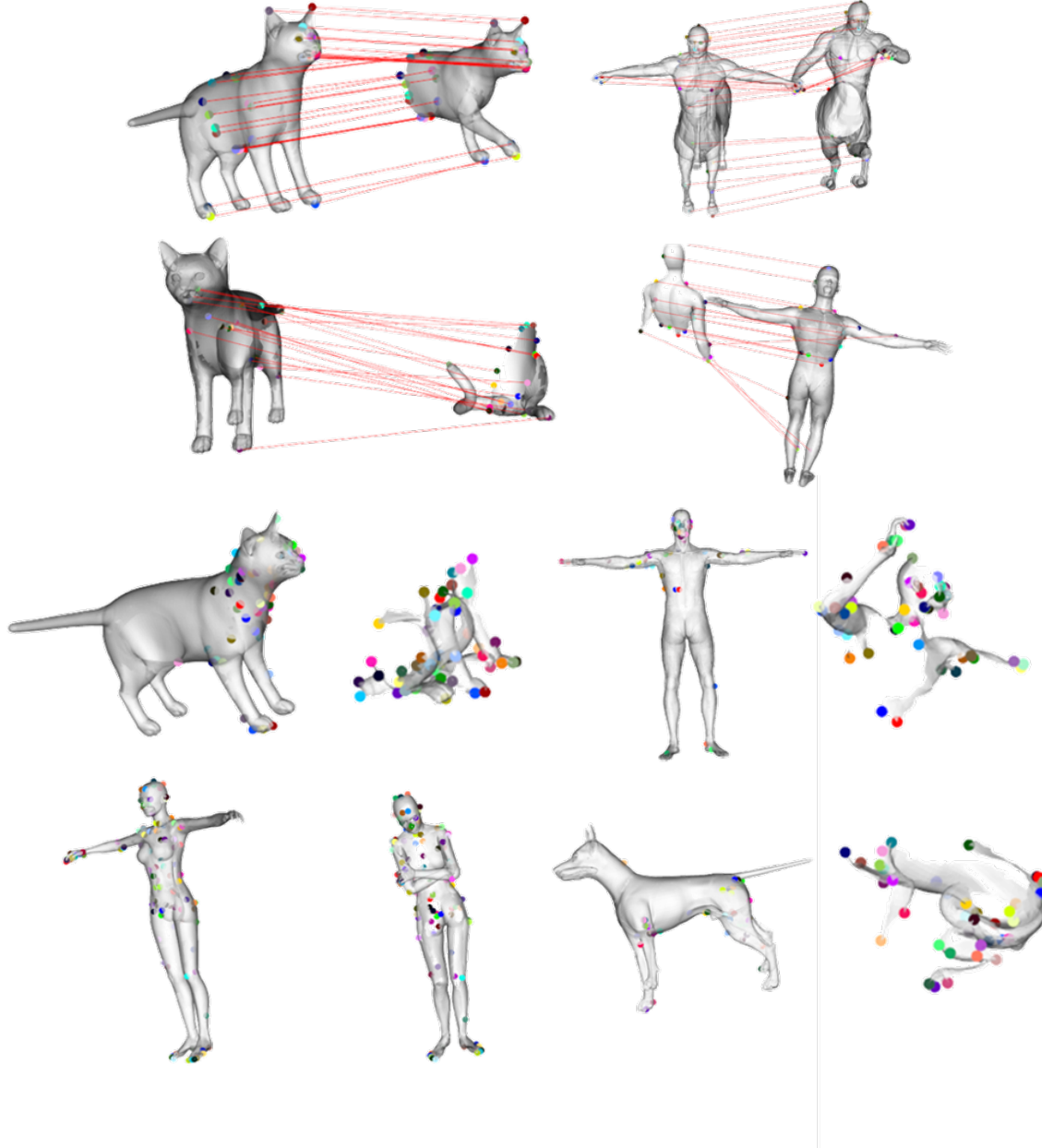


Figure 13. Some notable failure cases - most common is cat paw assignment - an extrinsic near symmetry gives rise to this phenomena. Closed fists on humanoids tends to cause a collapse of all fingers to a single finger. In the holes extreme partiality makes the geodesic distances break even over short distances.

1674
1675
1676
1677
1678
1679
1680
1681
1682
1683
1684
1685
1686
1687
1688
1689
1690
1691
1692
1693
1694
1695
1696
1697
1698
1699
1700
1701
1702
1703
1704
1705
1706
1707
1708
1709
1710
1711
1712
1713
1714
1715
1716
1717
1718
1719
1720
1721
1722
1723
1724
1725
1726
1727